[Title Page]

Novel Methods for Estimating Lithium-Ion Battery State of Energy and Maximum Available Energy

Linfeng Zheng[a,b,*], Jianguo Zhu[a], Guoxiu Wang[b], Tingting He[a], Yiying Wei[a,b]

a. Faculty of Engineering and Information Technology, University of Technology Sydney, Sydney, N.S.W., 2007, Australia

b. Centre for Clean Energy Technology, University of Technology Sydney, Sydney, N.S.W., 2007, Australia

*Corresponding author:

Linfeng Zheng, Faculty of Engineering and Information Technology, University of Technology Sydney, Sydney, N.S.W., 2007, Australia. Email: Linfeng.Zheng@student.uts.edu.au.

Novel Methods for Estimating Lithium-Ion Battery State of Energy and Maximum Available Energy

Abstract

The battery state of energy (SOE) allows a direct determination of the ratio between the remaining and maximum available energy of a battery, which is critical for energy optimization and management in energy storage systems. In this paper, the ambient temperature, battery discharge/charge current rate and cell aging level dependencies of battery maximum available energy and SOE are comprehensively analyzed. An explicit quantitative relationship between SOE and state of charge (SOC) for $LiMn_2O_4$ battery cells is proposed for SOE estimation, and a moving-window energy-integral technique is incorporated to estimate battery maximum available energy. Experimental results show that the proposed approaches can estimate battery maximum available energy and SOE with high precision. The robustness of the proposed approaches against various operation conditions and cell aging levels is systematically evaluated.

Key words: Battery management system (BMS); State of energy (SOE); State of charge (SOC); Maximum available energy.

1. Introduction

Lithium-ion batteries have many desirable merits such as high energy density, light weight and long cycle life, and are widely developed as energy storage devices in smart grids and electric vehicles [1,2], etc. To meet the application power and energy demands, a battery system usually contains hundreds, even thousands of cells connected in series and parallel. To ensure safe and reliable operation, an effective battery management system (BMS) is required to monitor and control these cells. Much of the BMS functionalities, such as the state of charge (SOC) estimation, state of health estimation, cell monitoring and balancing techniques [3-8], have been sophisticatedly developed for applications. Nevertheless, due to the nonlinear battery characteristics and unpredictable operating conditions, accurate and reliable battery state of energy (SOE) and maximum available energy estimations still pose significant challenges.

Traditionally, the SOC is regarded as an indicator of battery available energy. A wide variety of approaches for SOC estimation has been reported in recent literature [2,9-19], and remarkable results have been achieved on novel SOC estimation methods and improving the estimated accuracy. For example, the proportional-integral (PI) observer [11], Luenberger observer [12,13], Sliding-mode observer [14,15] and Kalman-filter-based algorithms [2,16-19] were employed in model-based SOC estimation methods to obtain estimated results of high accuracy. Defined as the ratio of the remaining charge stored in a battery to its full capacity, however, SOC actually indicates the state of available capacity rather than the state of available energy. K. Mamadou etc. [20,21]

introduced a new criterion, state of energy (SOE), for battery energetic performances evaluation. SOE allows a direct determination of the ratio of battery remaining energy to its maximum available energy, which is critical for energy optimization and management in energy storage systems.

Compared with the SOC estimation approaches, there are few studies report the systematic research for SOE estimation. Refs. [22,23] presented SOE estimation methods based on Neural Network, which treats the target battery as a "black-box" system and needs a great number of sample data to train the network parameters. The main disadvantage of this method is that the estimation errors are strongly dependent on the training data. In [24,25], an adaptive unscented Kalman filter algorithm and the relationship between the SOE and open circuit voltage (OCV) were employed in the model-based SOE estimation approaches. In [26], the particle filter and a battery model are utilized to develop a method for joint estimation of the SOE and the SOC, and the robustness of the method has been verified under dynamic temperature conditions. H. He etc. [27] employed a Gaussian model oriented battery model and proposed a data-driven estimator with a central difference Kalman filter algorithm for SOE estimation, and the approach was evaluated by two kinds of batteries including $LiFePO_4$ and $LiMn_2O_4$ cells. Although these SOE estimation approaches are able to achieve acceptable accuracy, the complex algorithms produce a heavy computational burden on the microprocessor with limited computation capability within BMSs.

Besides, a common drawback of these SOE estimation methods is that they fail to

61 achieve desirable predictions against various operating conditions during battery aging
62 processes. The trajectory of the neural network parameters or battery model parameters
63 cannot be fully described within a limited number of experiments [27]. Various battery
64 operating conditions and cell aging levels with pre-set parameters may lead to
65 inaccurate SOE estimated results. It is also noted that the above-mentioned battery
66 available energy studies focus just on the SOE estimation. Unfortunately, there are very
67 few studies involving the estimation of battery maximum available energy (i.e. battery
68 actual energy). Since the battery maximum available energy is strongly related to the
69 battery operating conditions [22], it is necessary to systematically study the effects of
70 ambient temperature, current rate, and aging level in order to estimate the SOE and
71 maximum available energy more accurately, and further improve the robustness of
72 estimation approaches against uncertain operating conditions.

73 To implement this work, a battery test bench was developed, and the characteristics of
74 $LiMn_2O_4$ battery cells with a nominal capacity of 90 Ah were tested under different
75 aging levels, current rates, and ambient temperatures. The tests cover a broad aging
76 level range from 92 Ah to 69.5 Ah, a wide temperature range from 10 °C to 40 °C and
77 a commonly used current rate range from 1/3 C to 1 C. Based on the test data, the
78 relationships between SOE and SOC under various operating conditions are
79 systematically analyzed and quantified for SOE estimation. A moving-window energy-
80 integral technique is incorporated to estimate the battery maximum available energy.
81 The robustness and feasibility of the proposed approaches are validated in different
82 operating condition tests during battery aging processes.

The remainder of the paper is arranged as follows: Section 2 introduces the battery test bench and analyzes the dependencies of battery available energy and SOE on the temperature, current and cell aging level. Section 3 presents the proposed algorithms of battery SOE and maximum available energy estimations. The experimental results and evaluation of the proposed approaches are reported in Section 4, followed by the conclusions and future work in Section 5.

2. Battery Experiments and Results

2.1. Battery Test Bench

The $LiMn_2O_4$ cells with a nominal capacity of 90 Ah were used to investigate the battery energy characteristics at various experimental conditions of different ambient temperatures, current rates, and cell aging levels. A battery test bench was set up to obtain battery characterization experimental data, as shown in Fig. 1.

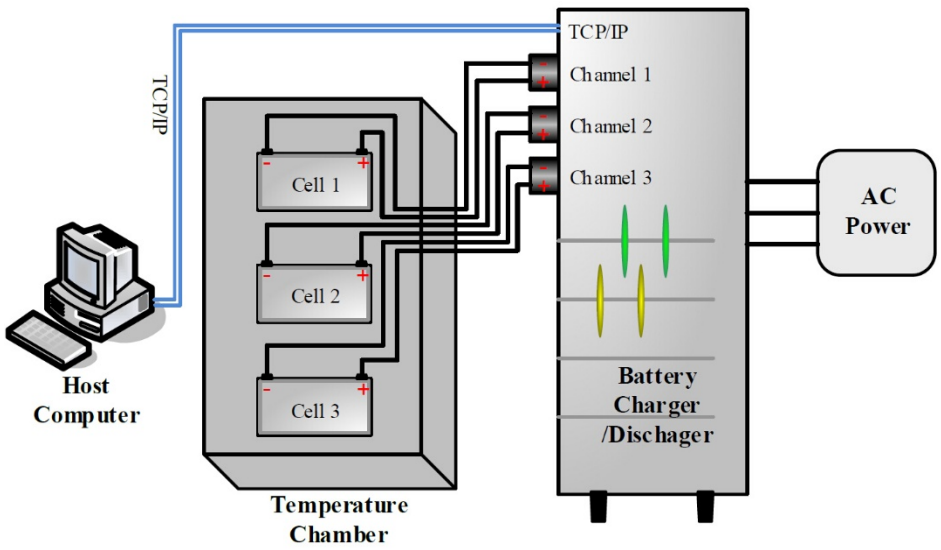

Fig. 1. Configuration of the battery test bench.

The battery test bench is composed of a battery charger/discharger, a host computer, a programmable temperature chamber and Lithium-ion battery cells. The battery charger/discharger functions to charge or discharge battery cells according to preset loading profiles and its voltage and current measurement accuracy is 0.05% full scale. The host computer is used to set the loading profiles and control the battery charger/discharger through the TCP/IP communications. It is also used to record a set of real-time battery variables, such as battery terminal voltage, loading current, and charge/discharge energy. The programmable temperature chamber can simulate various ambient temperatures and is used to control the battery operated under the designed temperatures.

2.2. Temperature, current and aging level dependencies of battery maximum available energy

In order to investigate the battery maximum available energy with different currents at various ambient temperatures, the battery cells were loaded with the discharge current rates of C/3, 2C/3, C/2 and 1C at temperatures of 10 °C, 25 °C and 40 °C, respectively. At each temperature, the battery cells were firstly charged with a preset constant current to the upper limit voltage 4.2 V followed by a constant voltage charge at 4.2 V until C/20 cutoff. Then, there was a rest time for 1 h followed by the preset constant current discharge to the lower limit voltage 3 V. After that, the battery was given a rest for 1 h and the procedure was carried out repeatedly. During the battery discharge processes, the maximum available energy results with different currents at various temperatures

are shown in Fig. 2.

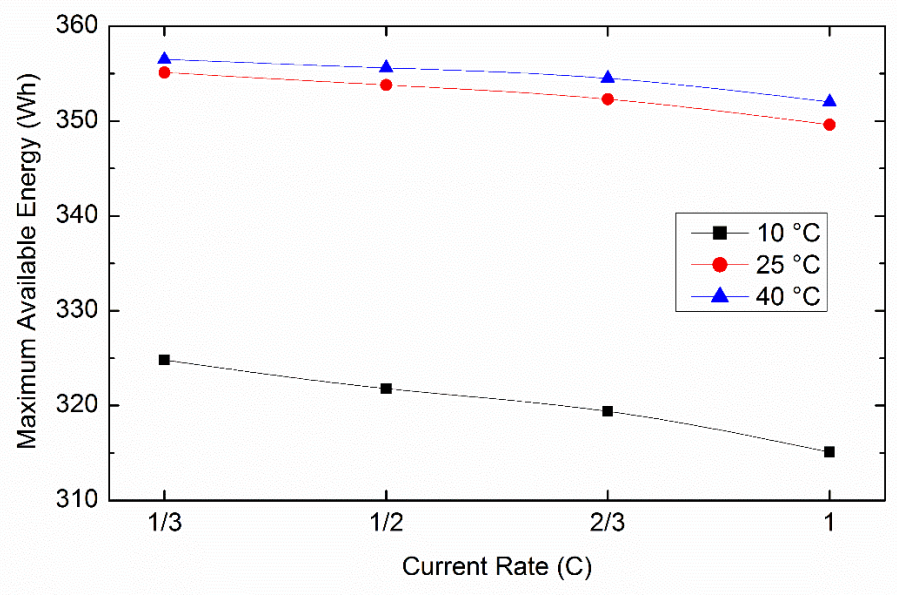

Fig. 2. The maximum available energy with different currents at various temperatures.

From Fig. 2, it can be found that the battery maximum available energy presents a change with different currents at various temperatures. At the same ambient temperature, the available energy appears a decreasing trend with the increasing discharge current rate. For example, when the discharge current rate was increased from 1/3C to 1C, the available energy dropped from 324.8 Wh to 315.1 Wh at 10 °C. At various temperatures, when the discharge current rate is kept at 1/3C, the maximum available energies are 324.8 Wh, 355.1 Wh, and 356.5 Wh at 10 °C, 25 °C and 40 °C, respectively, presenting an increasing trend with the rising temperature.

To investigate the battery maximum available energy with different currents at various battery cell aging levels, accelerated aging tests with the charge/discharge current of 1C at 60 °C were applied to the battery cell to obtain different cell aging levels including

92 Ah, 87 Ah, 82.5 Ah, 78 Ah, 74.5 Ah and 69.5 Ah, and at each cell aging level, the battery cell was loaded with the discharge currents of C/3, C/2, 2C/3 and 1C at the room temperature (25 °C), respectively. The battery maximum available energy values are plotted in Fig. 3.

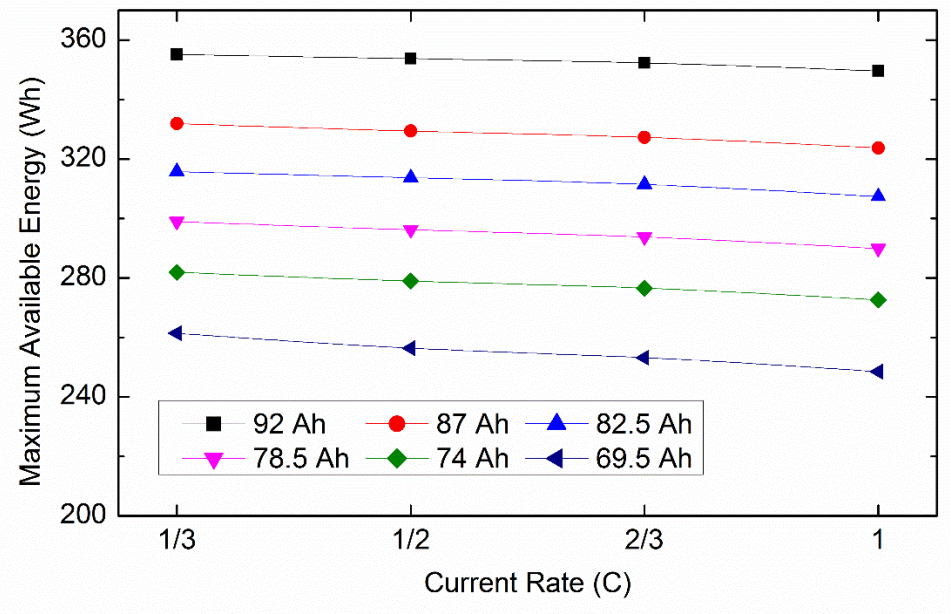

Fig. 3. The maximum available energy with different currents at various aging levels.

In Fig. 3, when the discharge current rate is 1/3C, the battery maximum available energy values are 355.1 Wh, 331.9 Wh, 315.8 Wh, 299.0 Wh, 281.9 Wh and 261.4 Wh at the battery capacity 92 Ah, 87 Ah, 82.5 Ah, 78.5 Ah, 74 Ah and 69.5 Ah, respectively. The maximum available energy shows similar declining trends with different discharge current rates such as 1/2C, 2/3C, and 1C at different aging levels, indicating that the battery maximum available energy appears a significant decrease during battery aging processes.

It can be concluded that the battery maximum available energy varies with the operating

conditions and is greatly related to the ambient temperature and cell aging level. Accordingly, it is necessary to develop reliable approaches for accurate battery maximum available energy and SOE estimations with strong robustness against the varying operating conditions during the battery aging processes.

2.3. Temperature, current and aging level dependencies of the relationship between SOE and SOC

Being similar to the SOC range, the SOE reaches its maximum value 100% when the battery is fully charged which means it has the maximum available energy, and it reaches its minimum value 0% when the battery is fully discharged which means there is not any remaining energy can be discharged. Since the battery charger/discharger is able to measure cell voltage and loading current with high precision, the referenced data are represented by the measurement data detected by the charger/discharger which are recorded in the host computer. The recorded data include the battery cell terminal voltage, loading current, charge/discharge capacity and energy, and therefore the SOC and SOE can be easily calculated by Eq. (1) and Eq. (2), respectively,

$$SOC(k)=SOC(k-1)+\eta_C I(k)\Delta t/C_a \tag{1}$$

$$SOE(k)=SOE(k-1)+U(k)I(k)\Delta t/E_a \tag{2}$$

where *SOC(k)* denotes the SOC value at time *k*, *SOC(k-1)* the SOC value at time (*k*-1), *SOE(k)* the SOE value at time *k*, *SOE(k-1)* the SOE value at time (*k*-1), Δt the sampling time interval, *I(k)* the loading current at time *k* (positive for charging and negative for

discharging), $U(k)$ the battery cell terminal voltage at time k, C_a the battery maximum available capacity (i.e. the battery actual capacity), E_a the battery maximum available energy (i.e. the battery actual energy), and η_C the coulombic efficiency which is considered to be approximately equal to 1 [26].

It has been reported that there is a positive correlation between the SOE and SOC [24], but the relationship between SOE and SOC has not been clearly defined. Thus, the relationship between SOE and SOC should be further studied. To investigate the temperature dependency of the relationship between SOE and SOC, different battery cells of the same batch were loaded with the discharge current C/3 at 10 °C, 25 °C and 40 °C, respectively. The relationships between SOE and SOC at different temperatures are plotted in Fig. 4 where the SOC is regarded as the X-axis and the SOE as the Y-axis.

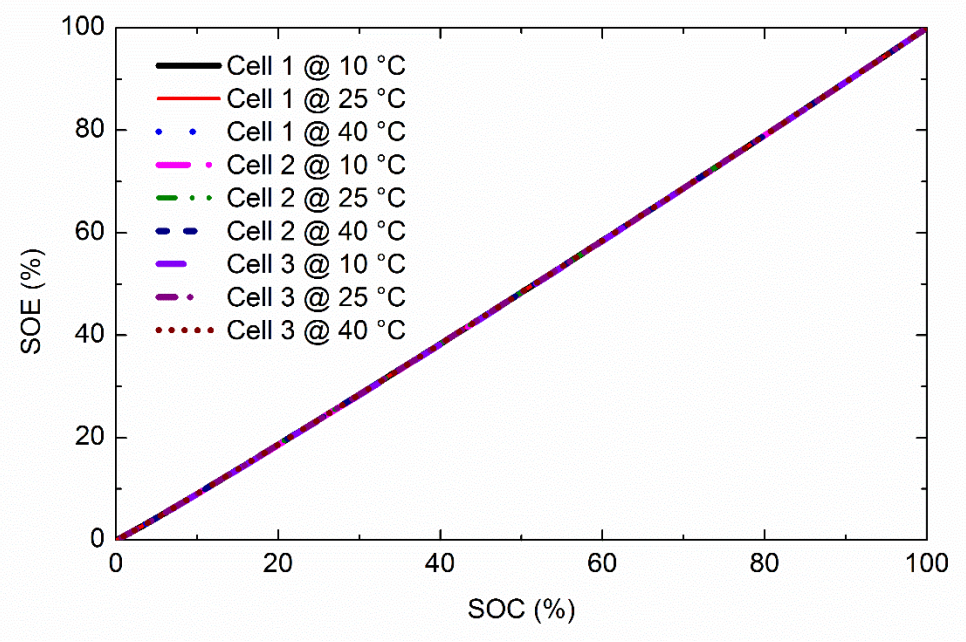

Fig. 4. The relationships between SOE and SOC at different temperatures.

Fig. 4 shows a perfect coincidence among the relationships between SOE and SOC at

different temperatures. It indicates that the relationship between SOE and SOC has strong robustness against the changing ambient temperature. Besides, it is noted that for three different cells of the same batch, the relationships between SOE and SOC also coincide well with each other. Thus, the relationship between SOE and SOC can be readily extended for each cell of whole battery pack operated at different ambient temperatures.

In order to investigate the current dependence of the relationship between SOE and SOC, the battery cells were loaded with the discharge and charge current rates of C/3, C/2, 2C/3 and 1C, respectively. The results are shown in Fig. 5.

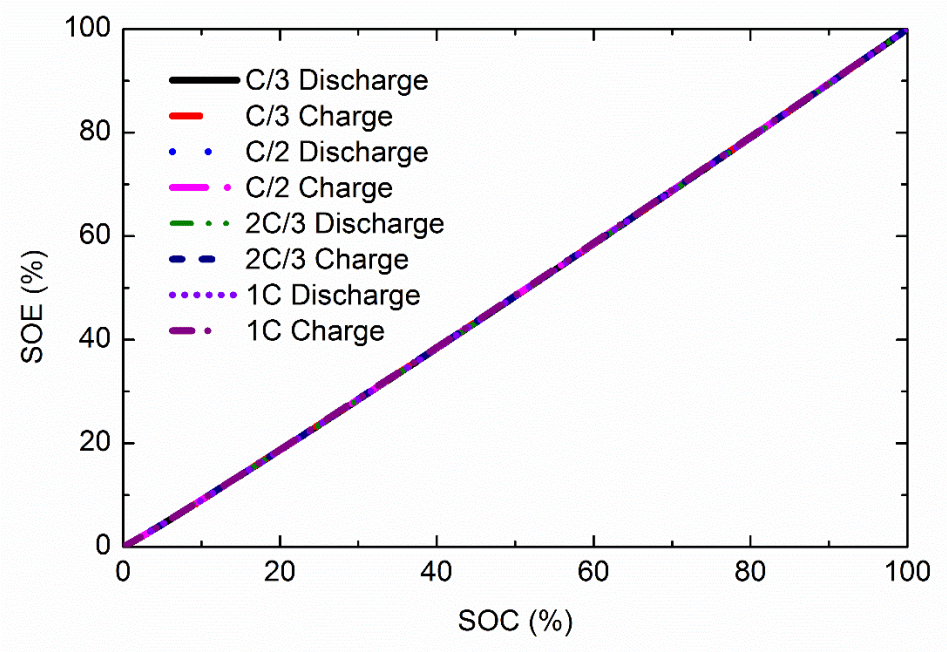

Fig. 5. The relationships between SOE and SOC with various current rates.

From Fig. 5, it can be seen that the relationships between SOE and SOC with various discharge or charge current rates almost coincide with each other. It manifests that the charging and discharging current rates have little effect on the relationship between

SOE and SOC. Thus, the relationship can be applied not only in battery constant current charging/discharging processes but also in dynamic changed current working conditions.

To investigate the aging level dependence of the relationship between SOE and SOC, the battery cell was loaded with a discharging current rate of C/3 at battery capacity degraded from 92 Ah to 69.5 Ah, respectively, and the relationships are shown in Fig. 6.

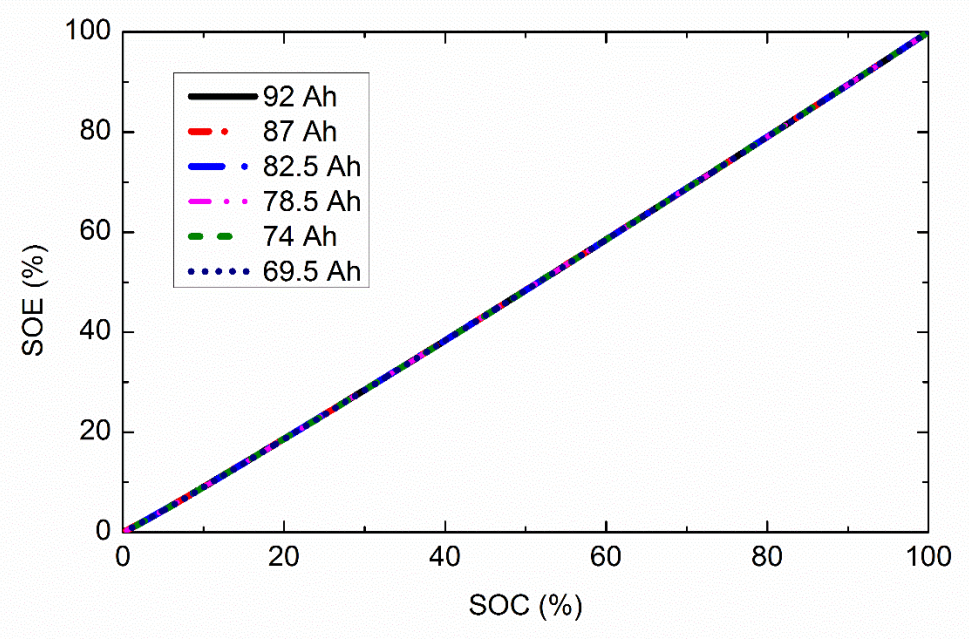

Fig. 6. The relationships between SOE and SOC at different aging levels.

In Fig.6, the relationships between SOE and SOC at different aging levels appear a superior overlapping characteristic. It demonstrates that the relationship between SOE and SOC remains steady during battery aging processes and has strong robustness against the battery capacity fade.

From above experimental results, it can be summarized that under different operating conditions and cell aging levels, the relationship between battery SOE and SOC always keeps unchanged. Although the maximum available energy and maximum available capacity of a battery cell are significantly dependent on its operated ambient temperature, loading current rate and aging level, it is noted that these factors have negligible effects on the relationship between SOE and SOC. This is because the SOE and SOC values were calculated by Eq. (1) and Eq. (2) with the maximum available energy and maximum available capacity, respectively, which have already included these influence factors.

3. The Proposed Algorithms

It has been reported that the model-based SOC estimation methods are able to achieve high estimated accuracy [9-19]. Thus, the estimated SOC and the stable relationship between SOE and SOC can be utilized to estimate SOE. According to the results shown in Figs. 4-6, the relationship between SOE and SOC can be expressed as an explicitly quantitative expression which is assumed to be a quadratic function, as given by,

$$SOE(k) = aSOC(k)^2 + bSOC(k) + c \tag{3}$$

where a, b and c are three coefficients of the quadratic function.

The coefficients of the quadratic equation are fit by using Levenberg-Marquardt algorithm [28,29] for the relationship between SOE and SOC under different temperatures, current rates, and cell aging levels. The optimal parameters are listed in

227 Table 1. The coefficient of determination *R-Square* is 0.999989, which means the fitting
228 function can precisely match the real relationship between SOE and SOC.

229

230 Table 1. Optimal parameters of the relationship function between SOE and SOC.

Parameter	Coefficient
a	0.000600
b	0.944954
c	-0.426930

231

232 Based on the quantitative relationship between SOE and SOC with estimation SOC, the
233 overall structure of the proposed algorithms for both battery SOE and maximum
234 available energy estimation is shown in Fig. 7.

235

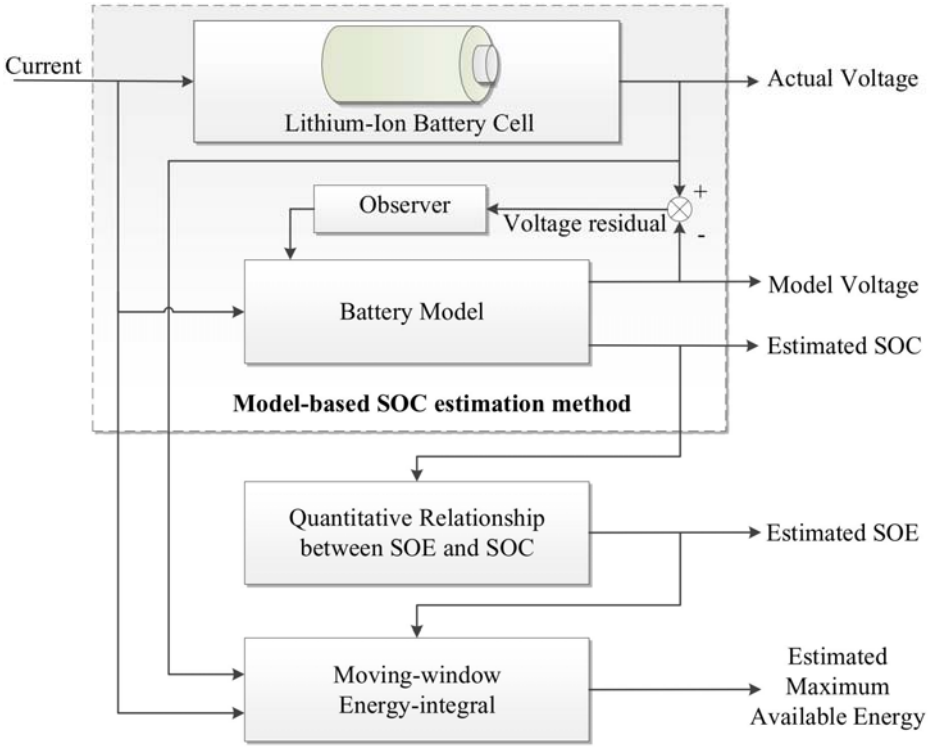

Fig. 7. The structure of the proposed algorithms.

The SOC is firstly estimated by a model-based estimation method. Since the model-based SOC estimation method is not the emphasis of this paper, we briefly explain the working principle of the method, and refer readers to Refs. [11-19,30] where give a more comprehensive description on the model-based SOC estimation methods. Briefly, a battery model such as equivalent circuit models and electrochemical models is employed to calculate the model output voltage with the given initial SOC value and loading current. Then the voltage residual between the model output voltage and the cell terminal voltage (i.e. cell actual voltage) is fed to an observer or filter such as PI observer, Luenberger observer, Sliding-mode observer and Kalman-filter-based filters, for producing a compensation value. After that, the compensation value is used to modify state variables of the battery model and therefore the estimated SOC is able to

249 track with the actual SOC.

250 Subsequently, the estimated SOC and the quantitative relationship are employed to
251 estimate SOE. Furthermore, a moving-window energy-integral technique with the SOE
252 estimation is incorporated to estimate the battery maximum available energy and its
253 detailed estimation process is described as follows.

254 Eq. (2) expresses the relationship between SOE and battery maximum available energy,
255 and therefore the battery maximum available energy can be derived reversely, as given
256 by,

257 $$E_a = \sum_{i=0}^{k} \left(U(i) I(i) \Delta t \right) / \left(SOE(k) - SOE(0) \right) \quad (4)$$

258 where $\sum_{i=0}^{k} \left(U(i) I(i) \Delta t \right)$ is the energy integral from the beginning time to the time k
259 and *SOE(0)* is the SOE value at the beginning time.

260 As mentioned in Section 2, the battery maximum available energy is greatly related to
261 the ambient temperature, cell aging level and loading current rate. However, it is noted
262 that these three variables are not included in Eq. (4). This is because that in Eq. (4), the
263 battery maximum available energy is calculated with the estimated SOE, which is
264 calculated by Eq. (3). Eq. (3) describes the quantitative relationship between SOC and
265 SOE, which was obtained by fitting the experimental SOC and SOE data under various
266 ambient temperatures, cell aging levels and loading current rates. From Figs. 4-6, it can
267 be seen that these variables have negligible effects on the relationship between SOE

and SOC. Thus, the variables are not included in Eq. (3) and also not included in Eq. (4). Since the SOC value is considered as the input for calculating the SOE given by Eq. (3) at different operating conditions, the SOC should be the value under the corresponding operating conditions, which has considered the variables of ambient temperature, cell aging level and loading current rate, and therefore the estimated SOE and maximum available energy values are also related to these variables.

As presented in Eq. (4), the battery maximum available energy can be calculated by using two certain SOE points such as the beginning charge/discharge point and the final charge/discharge point. However, the SOE estimation errors in these two points may lead to incorrect battery maximum available energy estimation results. From experience, one way to decrease the uncertainty in experimental data is to make multiple measurements and take the average. Accordingly, a moving-window energy-integral technique with multiple calculations is incorporated for the estimation. The battery maximum available energy is calculated in each 200 seconds' moving-window. Then the average of the maximum available energy values of each moving-window is considered as the final estimated result, as given by,

$$E_{a\_avg} = \sum_{i=1}^{n} E_{ai} \Big/ n \tag{5}$$

where E_{ai} is the maximum available energy in each moving-window and n the number of moving-windows.

4. Verification and Discussion

4.1. SOE estimation

As presented in our previous SOC estimation work [13], the SOC estimation error can be limited to a +/-2% error band and the estimated SOC can track with the referenced SOC quickly even with an erroneous initial SOC value. Combining the estimated SOC and the relationship between SOE and SOC, the SOE estimation result of a battery cell with 92 Ah and 1/3C discharging current rate is shown in Fig. 8 where the referenced SOE values are calculated by Eq. (2) with the experimental test data.

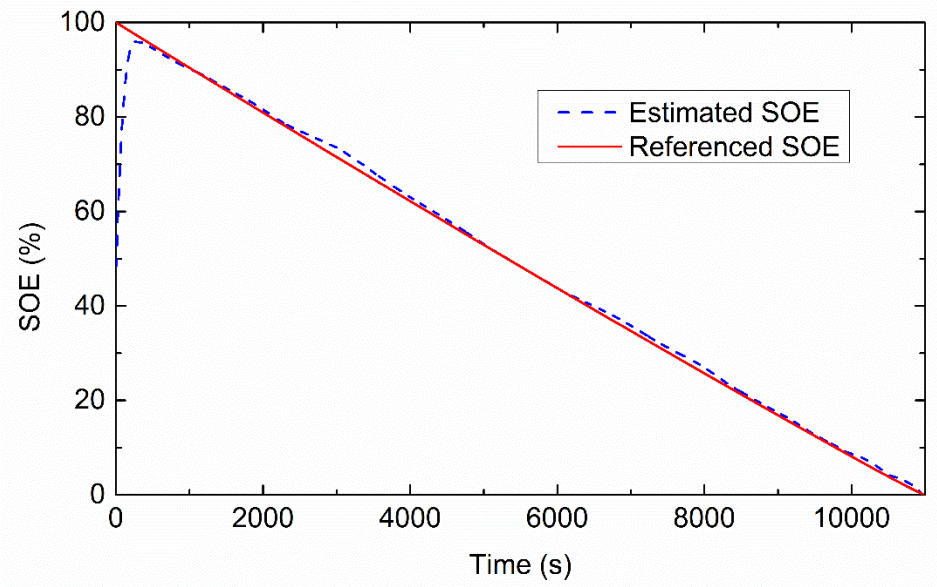

Fig. 8. SOE estimation result.

In Fig. 8, the referenced initial SOE value is 100% while there is an erroneous initial SOC value of the battery model that caused an incorrect initial SOE value 48%. It can be seen that in the first 400 s, the estimated SOE increases quickly to catch up with the referenced SOE, and therefrom the estimated SOE is able to follow the tracks of the

301 referenced value well. It indicates that the proposed SOE estimation method can work
302 well even when a grossly erroneous initial SOE value is supplied to the program. The
303 detailed SOE estimation errors at different battery aging levels and operation conditions
304 will be depicted as follows.

305 To investigate the effectiveness of the proposed method during the process of battery
306 aging, the battery cell degraded from 92 Ah to 69.5 Ah was used for the verification.
307 The SOE estimation errors including the maximum absolute error (MAE) and the root
308 mean square error (RMSE) are shown in Fig. 9 at six different aging levels with 92 Ah,
309 87 Ah, 82.5 Ah, 78.5 Ah, 74 Ah and 69.5 Ah, respectively.

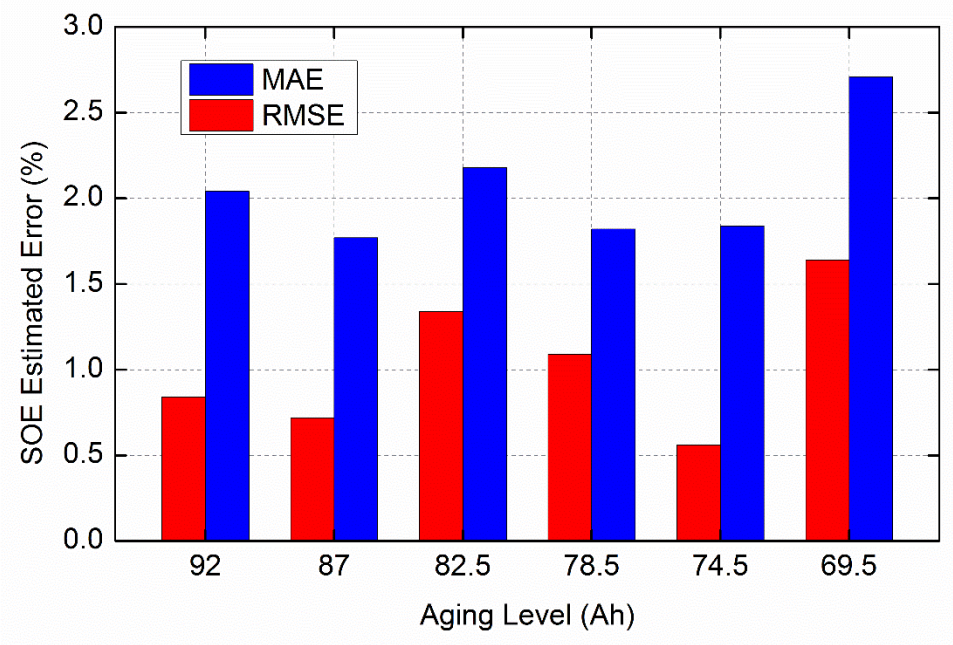

310

311 Fig. 9. SOE estimation errors at different battery aging levels.

312 In Fig. 9, the SOE estimation MAEs at different battery aging levels are less than 3.0%
313 while the SOE estimation RMSEs are less than 2.0%, indicating that the proposed
314 method can handle different battery aging levels quite well.

315 The characteristic test data at 10 °C, 25 °C and 40 °C were used to validate the
316 effectiveness of the proposed method under different ambient temperatures. The SOE
317 estimation errors are shown in Fig. 10.

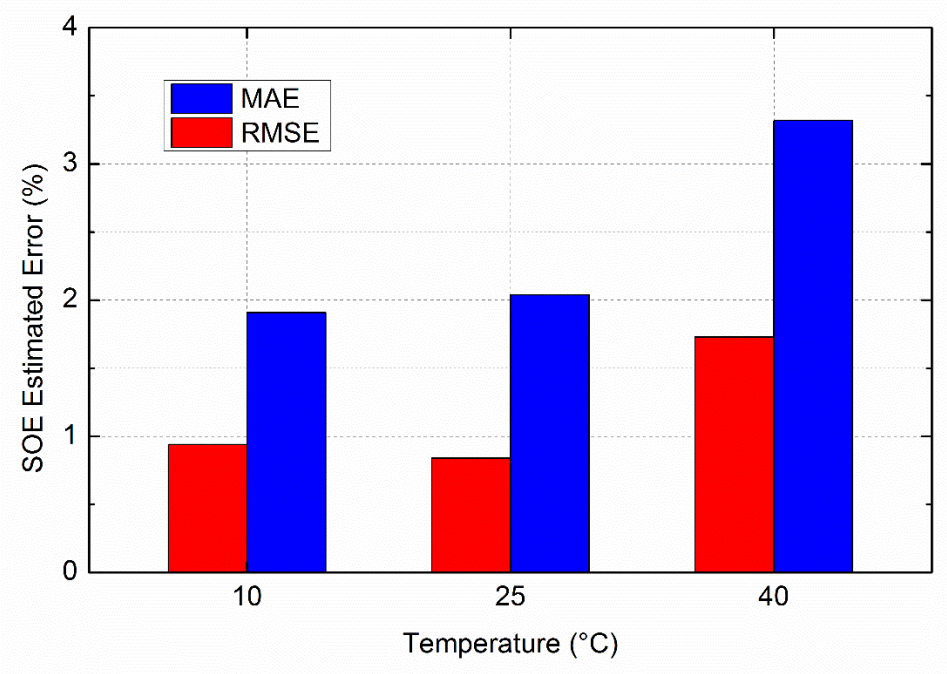

318

319 Fig. 10. SOE estimation errors under various ambient temperatures.

320 From Fig. 10, it can be seen that the maximum SOE estimation MAE occurred at 40 °C,
321 which is about 3.32%. At different ambient temperatures, the SOE estimation RMSEs
322 are less than 2.0%. It can be concluded that the proposed approach is able to achieve
323 desirable SOE estimation results under various ambient temperatures.

324 To investigate the effectiveness of the proposed method with different charge current
325 rates, the characteristic test data with four discharging current rates: 1/3C, 1/2C, 2/3C
326 and 1C at the room temperature (25 °C) were used to verify the method. The SOE
327 estimation errors are shown in Fig. 11.

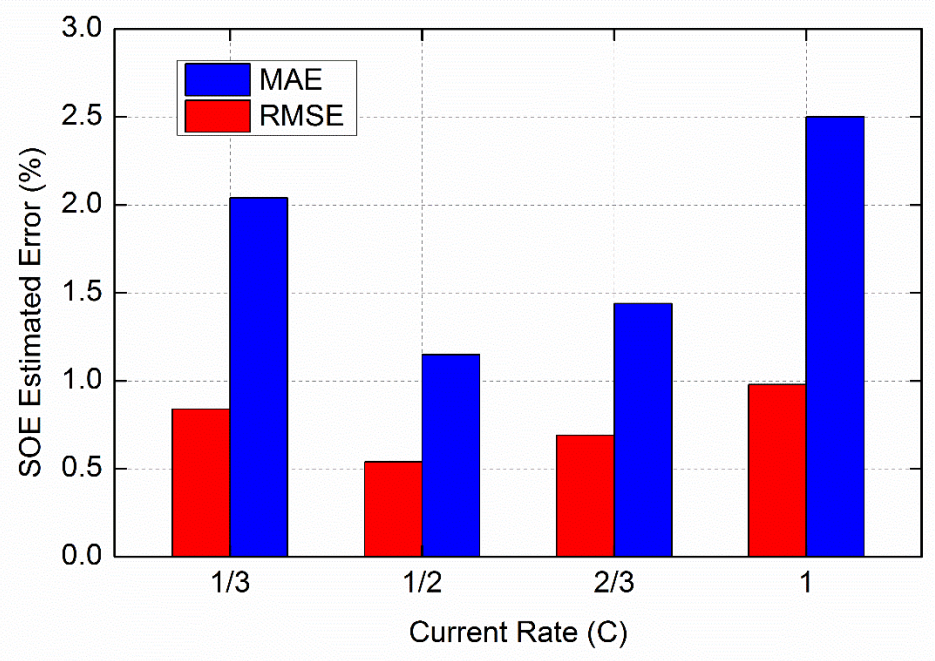

Fig. 11. SOE estimation errors with different discharge current rates.

In Fig. 11, the SOE estimation MAEs can be limited in a 2.5% error band and the SOE estimation RMSEs are less than 1.0% with different discharging current rates, indicating that the proposed approach can perform well with different discharge current rates.

4.2. Maximum available energy estimation

The battery maximum available energy is calculated by the proposed moving-window energy-integral and average methods. During the discharge process of a battery cell with 92 Ah and 1/3C discharging current rate, the maximum available energy estimation results are plotted in Fig. 12.

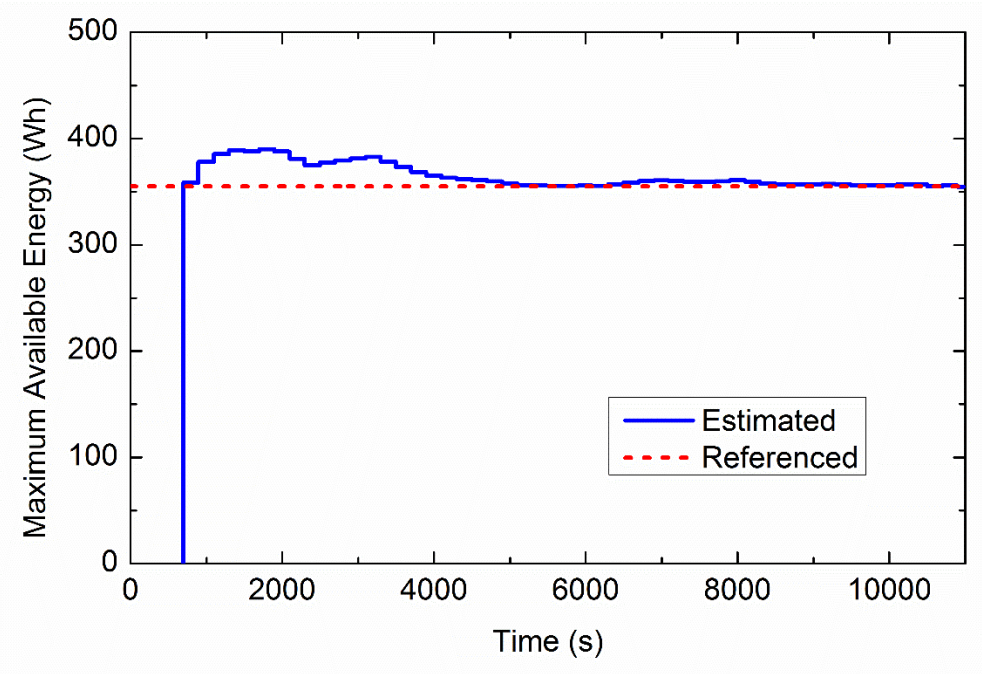

Fig. 12. Battery maximum available energy estimation results.

In Fig. 12, the proposed algorithm begins to estimate battery maximum available energy at about 700 s. This is because that the first 500 s are used for SOE estimation correction and the followed 200 s are used for the first moving-window calculation. Although some significant estimation errors occurred during the first 4000 s, the estimated maximum available energy can finally converge to the referenced value.

The battery test data at different aging levels are used to verify the effectiveness of the proposed method for battery maximum available energy estimation. The estimated results and relative estimation errors are shown in Fig. 13.

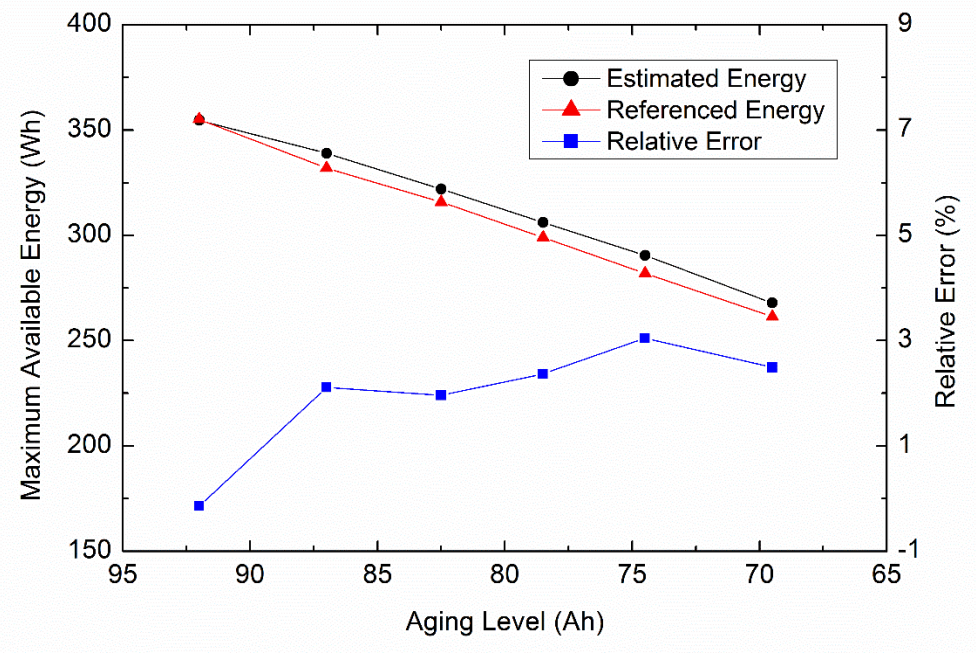

Fig. 13. Battery maximum available energy estimation results at different aging levels.

In Fig. 13, the estimated maximum available energies can track well with the referenced values at different battery aging levels, and the relative estimation errors can be limited in a +/-3% error band, indicating that the proposed method is feasible for various battery aging levels.

To verify the effectiveness of the proposed approach under different ambient temperatures, the estimated processes were performed at 10 °C, 25 °C and 40 °C, respectively, and the results are shown in Fig. 14.

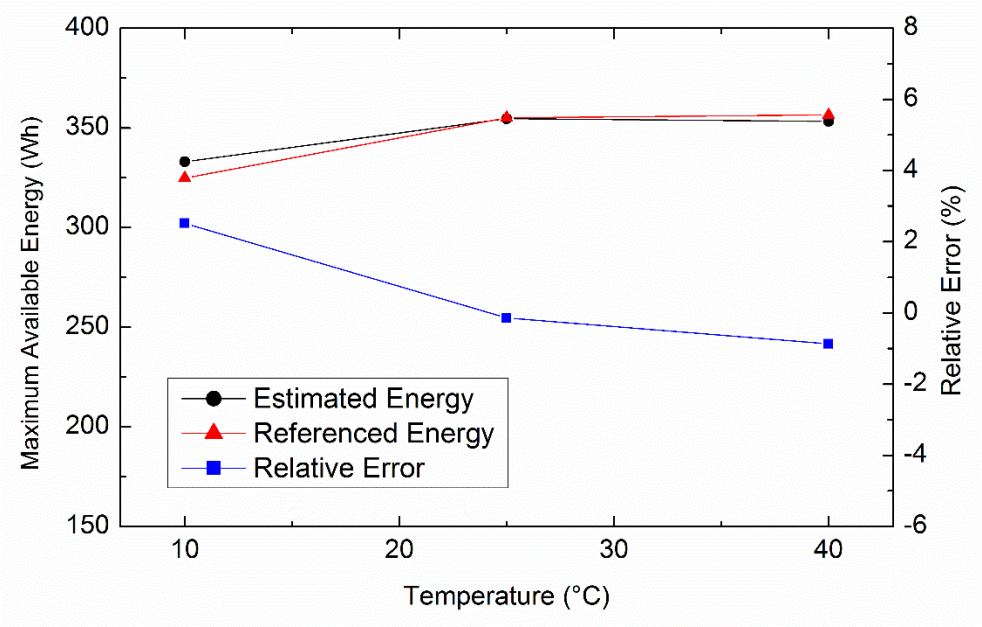

Fig. 14. Battery maximum available energy estimation results under different ambient temperatures.

Under various ambient temperatures, the estimated results presented in Fig. 14 show that the battery maximum available energy estimation method can work well at the above-mentioned temperatures and the relative estimation errors are able to be limited in a +/-2% error band.

To investigate the effectiveness of the proposed method with different charging current rates, the characteristic test data with four discharging current rates: 1/3C, 1/2C, 2/3C and 1C at the room temperature (25 °C) were used to verify the battery maximum available estimation, and the results are shown in Fig. 15.

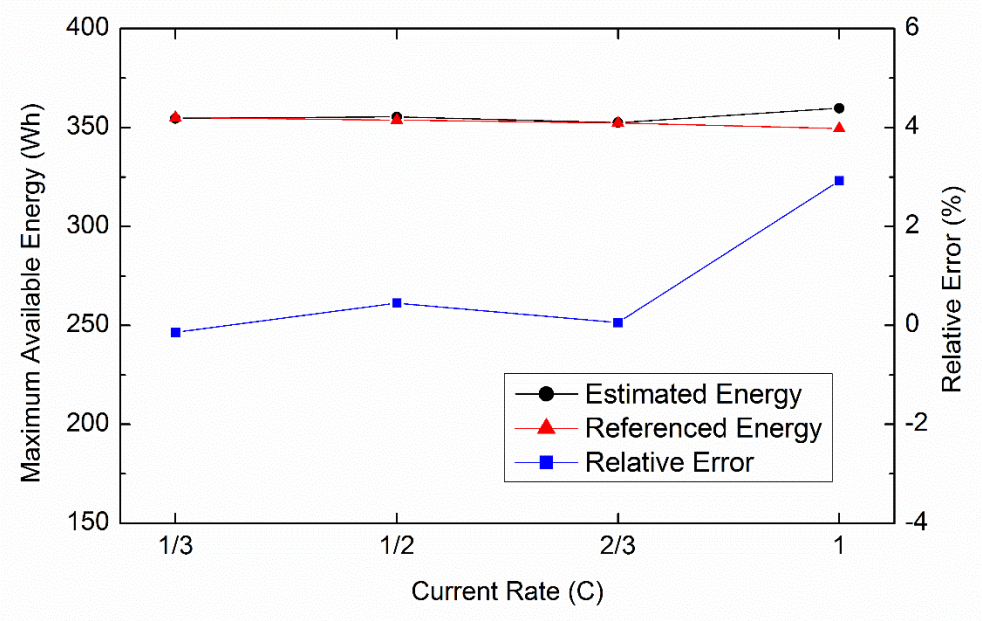

Fig. 15. Battery maximum available energy estimation results with different discharge current rates.

From Fig. 15, it can be seen that the estimated maximum available energies can follow the tracks of the referenced values well with different battery discharging current rates. The maximum estimated error is 2.92% at 1C current rate, showing that the proposed method can handle different discharging current rates quite well.

4.3. Dynamic stress test cycles verification

The dynamic stress test (DST) cycle [31] is widely used to simulate the dynamic changed loading conditions of batteries in real applications. The current profiles of DST cycles are depicted in Fig. 16(a). Before the DST test, the battery cell was fully charged in a constant current and constant voltage regime and the initial referenced SOE was 100% while the initial SOE of the algorithm was set to an incorrect value, 48%. The referenced SOE and the estimated SOE are compared in Fig. 16(b). It can be seen that

383 the estimated SOE is able to track the referenced value quickly. Fig. 16(c) shows the
384 estimated SOE errors, in which the SOE estimation MAE and RMSE are 3.2% and
385 1.2%, respectively. The battery maximum available energy estimation results are
386 plotted in Fig. 16(d). The resultant estimated maximum available energy is 324.2 Wh
387 in contrast to the referenced value of 331.9 Wh, and the relative error is 2.32%. The
388 estimated results indicate that the proposed methods can perform well with small errors
389 even under dynamic loading conditions.

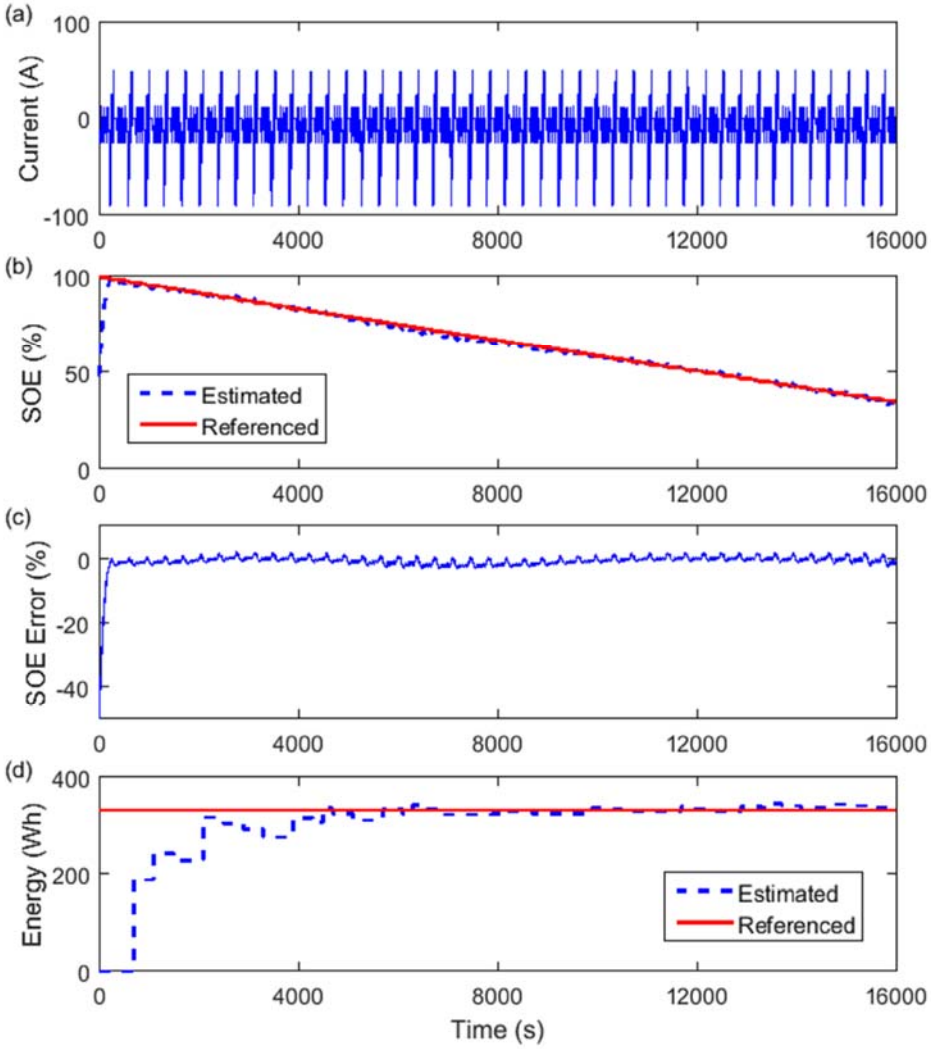

390

391 Fig. 16. Estimation results with DST cycles: (a) current profile of DST cycles, (b)

SOE estimated results, (c) SOE estimated errors and (d) maximum available energy estimated results.

5. Conclusion

Different from SOC, SOE allows a direct determination of the ratio of battery remaining energy to maximum available energy, which is critical for energy optimization and management in energy storage systems. In order to estimate the battery SOE and maximum available energy accurately, the temperature, current rate and battery aging level dependencies of battery maximum available energy and SOE were systematically analyzed. The relationships between SOC and SOE for different influence factors, such as the ambient temperature, charging and discharging current rates, and battery aging levels, were explicitly quantified for the SOE estimation. Besides, a moving-window energy-integral and average method were incorporated for battery maximum available energy estimation. Experimental results show that the proposed approaches can estimate the battery maximum available energy and SOE with high precision even under the dynamic loading conditions. The robustness of the proposed estimation approaches against various operation conditions and cell aging levels is systematically evaluated. The simplicity of the proposed SOE estimation method can avoid heavy computation cost required by conventional model-based SOE estimation methods, which causes a severe computational burden to the microprocessor with limited computation capability used in BMSs, and therefore the proposed method has the potential to be implemented in practical applications. Further work will be conducted

413 on the relationship between SOE and SOC and estimation of SOE and maximum
414 available energy for other types of batteries.

415 **Acknowledgment**

416 This work was financially supported by the Automotive Australia 2020 Cooperative
417 Research Centre (AutoCRC). The authors would also like to acknowledge the National
418 Active Distribution Network Technology Research Center (NANTEC), Beijing
419 Jiaotong University, for the prior work on battery tests.

420 **References**

421 [1] Su W, Eichi H, Zeng W, Chow M. A survey on the electrification of transportation
422 in a smart grid environment. Industrial Informatics, IEEE Transactions on 2012;8:1-10.

423 [2] He H, Xiong R, Peng J. Real-time estimation of battery state-of-charge with
424 unscented Kalman filter and RTOS μCOS-II platform. Appl Energy 2016;162:1410-8.

425 [3] Rahimi-Eichi H, Ojha U, Baronti F, Chow M. Battery management system: An
426 overview of its application in the smart grid and electric vehicles. Industrial Electronics
427 Magazine, IEEE 2013;7:4-16.

428 [4] Lu L, Han X, Li J, Hua J, Ouyang M. A review on the key issues for lithium-ion
429 battery management in electric vehicles. J Power Sources 2013;226:272-88.

430 [5] Wang L, Pan C, Liu L, Cheng Y, Zhao X. On-board state of health estimation of
431 LiFePO 4 battery pack through differential voltage analysis. Appl Energy
432 2016;168:465-72.

433 [6] Kim H, Shin KG. DESA: Dependable, efficient, scalable architecture for
434 management of large-scale batteries. Industrial Informatics, IEEE Transactions on
435 2012;8:406-17.

436 [7] Wang S, Shang L, Li Z, Deng H, Li J. Online dynamic equalization adjustment of
437 high-power lithium-ion battery packs based on the state of balance estimation. Appl
438 Energy 2016;166:44-58.

[8] Park H, Kim C, Park K, Moon G, Lee J. Design of a charge equalizer based on battery modularization. Vehicular Technology, IEEE Transactions on 2009;58:3216-23.

[9] Barillas JK, Li J, Günther C, Danzer MA. A comparative study and validation of state estimation algorithms for Li-ion batteries in battery management systems. Appl Energy 2015;155:455-62.

[10] Zhong L, Zhang C, He Y, Chen Z. A method for the estimation of the battery pack state of charge based on in-pack cells uniformity analysis. Appl Energy 2014;113:558-64.

[11] Xu J, Mi CC, Cao B, Deng J, Chen Z, Li S. The state of charge estimation of lithium-ion batteries based on a proportional-integral observer. Vehicular Technology, IEEE Transactions on 2014;63:1614-21.

[12] Hu X, Sun F, Zou Y. Estimation of state of charge of a lithium-ion battery pack for electric vehicles using an adaptive Luenberger observer. Energies 2010;3:1586-603.

[13] Zheng L, Jiang J, Wang Z, Zhao T, He T. Embedded implementation of SOC estimation based on the Luenberger observer technique. 2014:1-4.

[14] Kim I. The novel state of charge estimation method for lithium battery using sliding mode observer. J Power Sources 2006;163:584-90.

[15] Kim I. A technique for estimating the state of health of lithium batteries through a dual-sliding-mode observer. Power Electronics, IEEE Transactions on 2010;25:1013-22.

[16] Xiong R, Sun F, Chen Z, He H. A data-driven multi-scale extended Kalman filtering based parameter and state estimation approach of lithium-ion olymer battery in electric vehicles. Appl Energy 2014;113:463-76.

[17] Plett GL. Extended Kalman filtering for battery management systems of LiPB-based HEV battery packs: Part 1. Background. J Power Sources 2004;134:252-61.

[18] Plett GL. Extended Kalman filtering for battery management systems of LiPB-based HEV battery packs: Part 2. Modeling and identification. J Power Sources 2004;134:262-76.

[19] Plett GL. Extended Kalman filtering for battery management systems of LiPB-based HEV battery packs: Part 3. State and parameter estimation. J Power Sources 2004;134:277-92.

471 [20] Mamadou K, Delaille A, Lemaire-Potteau E, Bultel Y. The state-of-energy: A new
472 criterion for the energetic performances evaluation of electrochemical storage devices.
473 ECS Transactions 2010;25:105-12.

474 [21] Mamadou K, Lemaire E, Delaille A, Riu D, Hing S, Bultel Y. Definition of a state-
475 of-energy indicator (SoE) for electrochemical storage devices: application for energetic
476 availability forecasting. J Electrochem Soc 2012;159:A1298-307.

477 [22] Liu X, Wu J, Zhang C, Chen Z. A method for state of energy estimation of lithium-
478 ion batteries at dynamic currents and temperatures. J Power Sources 2014;270:151-7.

479 [23] Dong G, Zhang X, Zhang C, Chen Z. A method for state of energy estimation of
480 lithium-ion batteries based on neural network model. Energy 2015;90:879-88.

481 [24] Zhang W, Shi W, Ma Z. Adaptive unscented Kalman filter based state of energy
482 and power capability estimation approach for lithium-ion battery. J Power Sources
483 2015;289:50-62.

484 [25] Liu HW, Wang HF, Guo C. State of energy estimation based on AUKF for lithium
485 battery used on pure electric vehicle. 2013;608:1627-30.

486 [26] Wang Y, Zhang C, Chen Z. A method for joint estimation of state-of-charge and
487 available energy of LiFePO 4 batteries. Appl Energy 2014;135:81-7.

488 [27] He H, Zhang Y, Xiong R, Wang C. A novel Gaussian model based battery state
489 estimation approach: State-of-Energy. Appl Energy 2015;151:41-8.

490 [28] Moré JJ. The Levenberg-Marquardt algorithm: implementation and theory. In:
491 Anonymous Numerical analysis: Springer; 1978, p. 105-116.

492 [29] Khan MR, Mulder G, Van Mierlo J. An online framework for state of charge
493 determination of battery systems using combined system identification approach. J
494 Power Sources 2014;246:629-41.

495 [30] Han X, Ouyang M, Lu L, Li J. Simplification of physics-based electrochemical
496 model for lithium ion battery on electric vehicle. Part II: Pseudo-two-dimensional
497 model simplification and state of charge estimation. J Power Sources 2015;278:814-25.

498 [31] United States Advanced Battery Consortium. Electric vehicle battery test
499 procedures manual. USABC, Jan 1996.

500